Prediction of thermal behaviors of an air-cooled lithium-ion battery system for hybrid electric vehicles

CrossMark

Yong Seok Choi[*], Dal Mo Kang

Battery R&D, LG Chem/Research Park, Daejeon 305-380, Republic of Korea

HIGHLIGHTS

- A methodology for modeling thermal behavior of HEV battery system is proposed.
- Use of internal resistance depending on SOC and temperature shows accurate prediction.
- Proper air channel width and amount of coolant flow rate are derived for flow system.

ARTICLE INFO

ABSTRACT

Thermal management has been one of the major issues in developing a lithium-ion (Li-ion) hybrid electric vehicle (HEV) battery system since the Li-ion battery is vulnerable to excessive heat load under abnormal or severe operational conditions. In this work, in order to design a suitable thermal management system, a simple modeling methodology describing thermal behavior of an air-cooled Li-ion battery system was proposed from vehicle components designer's point of view. A proposed mathematical model was constructed based on the battery's electrical and mechanical properties. Also, validation test results for the Li-ion battery system were presented. A pulse current duty and an adjusted US06 current cycle for a two-mode HEV system were used to validate the accuracy of the model prediction. Results showed that the present model can give good estimations for simulating convective heat transfer cooling during battery operation. The developed thermal model is useful in structuring the flow system and determining the appropriate cooling capacity for a specified design prerequisite of the battery system.

1. Introduction

Until now, nickel-metal hydride (NiMH) battery systems have been the major sources of electric propulsion and power storage for hybrid electric vehicles (HEV) in the market. As the technology matures, needs for more compact and lighter battery system have increased to achieve more efficient vehicle design. To save the space in the vehicle for better space utilization and reduce the battery weight for better efficiency, the demand for lithium-ion (Li-ion) battery systems has been increased due to their distinct advantages over NiMH in many aspects. Li-ion batteries have about 50% higher specific energy or mass density than NiMH [1,2]. Also, they are better in terms of such characteristics as self-discharge and lack of memory effect [3,4] allowing better lifetime-related characteristics

than other forms of secondary batteries such as nickel–cadmium based ones. For these reasons, major automakers and battery providers have been developing systems using Li-ion batteries for high power HEV applications. Over the past few years, companies and research institutes have shown the feasibility of using Li-ion batteries for HEV applications [5–9].

One of the issues with the Li-ion batteries is that they are more vulnerable to over-heating than NiMH batteries. The cycle life of Li-ion battery will also decrease dramatically under high temperature environments [10–12]. If the Li-ion battery system is stored and/or operated at a certain high temperature, the specific battery cell in the system may degrade faster than others kept and operated at a lower temperature. When a single cell in the system (battery pack) degrades faster than others in the same pack, the system's performance will be restricted mainly by the performance of the most degraded cell. This cell will break the electrical balance among cells, and the power output from the battery system can significantly be reduced. This degraded cell may induce, due to the increased

* Corresponding author. Tel.: +82 42 866 2636; fax: +82 42 862 1981.
  E-mail address: cysuk2002@gmail.com (Y.S. Choi).

internal resistance, even higher local temperature distribution. For this reason, it is important to reduce the temperature spread among cells in the battery pack as low as possible while it is also important to keep the maximum temperature of the cell in the battery pack lower than a certain target value. Here, the target maximum temperature is defined in accordance with the cycle life and calendar life characteristics of the cells to meet the typical lifetime standard of vehicle components.

If the temperature of the battery cell is raised even higher, the electrolyte inside may gasify and build up pressure inside the cell. And eventually gas-vent may occur [13,14] due to the elevated pressure inside the cell. This event may cause serious safety issues that an appropriate device or mechanism should be devised to avoid critical events. Here, one of the advantages of laminated film packaged cells (pouch cell) over prismatic-type or cylindrical-type battery cells is that the laminated packaged cells do not explode since the pressure build-up inside the cells is relatively lower.

Regarding the thermal management design of cells and systems, efforts have been made in various ways. Thermal models were set-up and simulated [5,15] and contributions of each components of cells such as electrodes and electrolytes were also modeled [16]. Use of transformer coolants [17] and phase change materials [18] were proposed for system level thermal management designs, which were not very realistic to be applied to real world systems due to the lack of cost effectiveness and complexity of structures. Scaled-up battery model simulations were made [19,20], though these analyses were more concerned on the cell side, not being able to fully access the full-system level thermal management.

A diagram shown in Fig. 1 describes how items to be considered for a successful design of HEV battery systems are interrelated with each other. The cells satisfying basic characteristics required by HEVs, such as high discharge power, large capacity, long enough cycle/calendar life, and cold cranking power outputs, are to be developed first. For the current system, Li-ion battery cells with high power and capacity have been developed and

introduced [6]. Based on the cell's electrochemical, mechanical, and electrical characteristics, a structure is designed. The thermal management system (TMS) is an invisible but an important part of the system consisting of coolant flow structure and the fan control strategy. During the thermal design phase the flow channel sizes and shapes inside the battery system are optimized for the given number of cells. The battery power cycles are defined in accordance with the HEV system strategies, and used for the optimization process. The other items in Fig. 1 describe the test and manufacturing phase of the battery system developments.

The purpose of this work is to propose a suitable thermal model for predicting air-cooled Li-ion HEV battery systems' thermal behavior and to show this model can give good approximations for use in real world HEV design processes. The model is developed from proper heat transfer assumptions and then model predictions are validated by comparing with test results based on vehicle driving schedule. Using the model, estimations of proper amount of coolant air flow rate and flow channel size are possible, which gives a guideline to the early design phase of the battery system.

2. Simulation model

2.1. Heat transfer model of the HEV battery system

A complete heat transfer model consists of all three possible heat transfer modes – conduction, convection, and radiation. In designing a thermal model for the current HEV battery system, however, the model can be simplified by making appropriate assumptions.

A basic structure of the HEV battery system for the present study is shown in Fig. 2. The section A is the coolant (air) inlet and B the outlet. The coolant air travels through the system by entering at section A then branches into many channels to meet at the bottom section of the duct and exits at section B (U-type flow). The heat transfer occurs mainly by the interaction of the sub-streams (C) and the blocks (D) that define the sub-stream channels. The blocks providing coolant channel walls for the sub-streams are the battery cells, the source of heat. For the present battery system one block is comprised of two cells and exposed to the coolant flow for heat transfer. Here, one surface per cell is exposed to the coolant flow for cooling by convective heat transfer. These blocks are not contacting with significant contact area to the system's frame and even this little amount of contact is through plastic housing, which implies the amount of heat transferred from the cell to the outside structure via conduction can be ignored. Thus conduction was not considered here.

The air channel (C) is a narrow path through which the coolant air flows. The width of the channels is set to 2 mm for the present model. The surrounding and opposing walls around the air channels are assumed to be heated by the battery cells. Under this
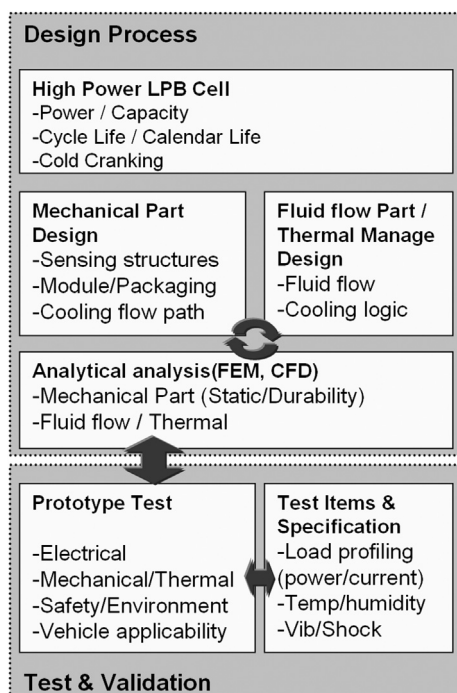

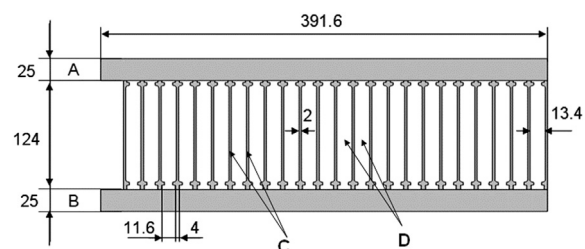**Fig. 1.** Items to be considered during the design phase of HEV battery system.
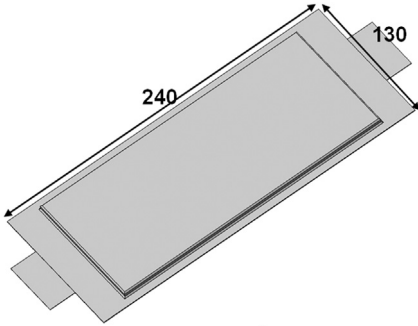

Fig. 2. Flow structure of the system; A – the coolant inlet, B – the outlet, C – flow channels (sub-streams), D – two-cell units (heat generating body). All dimensions in millimeters.

environment, radiation heat transfer is also negligible since the view factor to the low temperature outside from the surface of the cell is negligibly small, and the radiation to and from the surrounding walls (with large view factors) is not significant since the surface temperatures of the walls were assumed to be about the same. So for the current analysis only the convection heat transfer was considered.

2.2. Heat generation from the battery cell

The battery cell used for this analysis is a laminated film packaged Li-ion polymer cell for HEV applications. To complete the battery system, 48 cells were connected in series to deliver high voltage. The shape and basic performance specifications of the cell are shown in Fig. 3. And, essential for thermal modeling, the internal resistance of the cell was measured with direct current power and resistance (DCPR). The internal resistance is a function of state of charge (SOC), cell temperature, charge/discharge status, and pulse duration. Values shown in Table 1 are 10-s direct current internal resistance values. Cell level hybrid pulse power characterization (HPPC) test according to the FreedomCAR power-assist battery test manual [21] was conducted to obtain the cell internal resistance at various SOC and temperatures. The magnitude of pulse current during the test was 60 A.

Heat is generated intrinsically in Li-ion battery cells during their usage. Based on the energy balance around the cell control volume, primary sources of heat are originated from the overpotential due to ohmic losses, charge transfer overpotential, mass transfer limitation, and entropic heat [22]. The mass transfer effect is apparent under long discharge cycles that the depth of discharge (DOD) gets close to the maximum (100%) or under high current (C-rate) cycles, while the entropic effect is important under low C-rate applications. One interesting feature about the entropic effect is that it is either an endothermic or exothermic event depending on the SOC [23]. And for the pulse current test or charge sustaining (CS) cycles where the SOC is kept within the narrow range, the entropic heat is generally discarded. In most HEV applications, the typical SOC window is between 30 and 70% or narrower than this depending on the vehicle strategy. Thus the entropic heat was excluded in this work. Then remaining heats

Table 1
10 sec direct current internal resistance of the cell vs. temperature and SOC under charge and discharge conditions.

SOC (%)	Charge internal resistance (mΩ)				Discharge internal resistance (mΩ)			
	20	40	60	80	20	40	60	80
Temperature								
0 °C	17.1	15.9	14.3	11.9	17.3	16.1	15.2	14.5
10 °C	9.4	8.5	7.4	7.5	9.3	8.6	7.7	7.5
25 °C	4.7	4.3	3.7	3.8	4.8	4.3	3.8	3.6
35 °C	3.8	3.3	2.8	2.8	3.8	3.4	2.9	2.7
45 °C	3.2	2.7	2.3	2.3	3.2	2.9	2.3	2.2

can be expressed as an overpotential term as follows to calculate overall heat generation [24].

$$q_{gen} = I(U - V) = I^2 \cdot iR_{cell}, \tag{1}$$

where I is the current flowing through the battery cell, U the open circuit voltage, V the cell voltage, and iR_{cell} the direct current internal resistance of battery cells. Here, iR_{cell} can be expressed as a function of four variables, as previously mentioned, defining the cells' operating conditions.

$$iR_{cell}^t = iR_{cell}\left(CDS^t, \tau^t, SOC^{t-1}, T_{cell}^{t-1}\right), \tag{2}$$

where CDS indicates charge/discharge state of the battery, τ the charge or discharge pulse duration up to time t, and T_{cell} the cell temperature. Here, 't' indicates the current time.

If the battery is kept under the same charge or discharge condition at time $t + 1$, the pulse duration increases, so the internal resistance is updated by Eq. (3).

$$iR_{cell}^{t+1} = iR_{cell}\left(CDS^t, \tau^{t+1} = \tau^t + \Delta t, SOC^t, T_{cell}^t\right), \tag{3}$$

where Δt is the time step for simulations.

2.3. Lumped thermal model

Two-cell units shown in Fig. 4 are composed of two battery cells attached together and are, hereafter, to be considered the
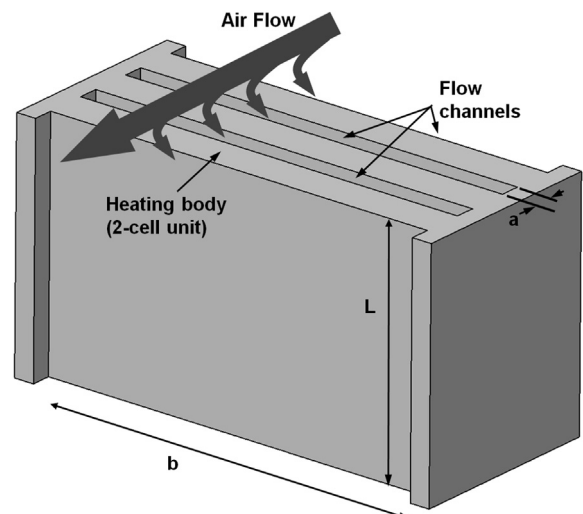

Cell Characteristics		
1C Capacity	Nominal	6.0 Ah
Dimensions	Thickness	6.5 mm
	Width	130.0 mm
	Height	240.0 mm
Weight (Typical)		300 g
Nominal Voltage		3.7 V

Fig. 3. Cell characteristics used for the current analysis.

Fig. 4. A simplified coolant flow structure of the system for the lumped thermal model ($a = 2$ mm, $b = 210$ mm, $L = 124$ mm).

only heat source. For the present batter system a total of 24 two-cell units were positioned horizontally with equal spacing between them. The coolant air is directed in through an inlet, travels above the top of the two-cell unit arrays, then, divided into substreams to pass through the channels between two-cell units to cool down the battery cells via convection heat transfer. Heated air is collected at the bottom and expelled through an outlet by a blower.

Based on the simplification of the system in Fig. 4, a heat transfer model of the internal flow through ducts with rectangular cross-section can be applied to predict the system's thermal behavior. In this model, walls ($L \times b$) defined by the two-cell units are the heating surfaces, and the other areas and boundaries are considered thermally insulated. So the number of heating surfaces (the heat transfer surfaces) is one per each cell, and $L \times b$ is the area of the cooling surface per cell. The size of each air channel is $a \times b$, and this channel was considered the only path for the coolant air. A single channel was analyzed with the assumption that the flow rate through each channel is the same for all channels that the flow rate for a single channel is given by the total flow rate through the battery system divided by the number of air channels. This assumption is a very important one to be experimentally and/or numerically validated since the distribution of flow among air channels is what determines the cell temperature distribution within the battery system. Much effort has been taken to optimize this flow distribution by numerical and experimental approach.

The amount of heat accumulated on the cells is the heat generation subtracted by the amount of heat rejected. Energy conservation in the transient state yields.

$$m_{\text{cell}}C_{p,c}\frac{\mathrm{d}T_{\text{cell}}}{\mathrm{d}t} = q_{\text{gen}} - q_r, \tag{4}$$

Here, m_{cell} is the mass of the cell in the system, $C_{p,c}$ the specific heat capacity of the cell obtained from transient temperature measurement [25], q_{gen} the amount of heat generation, and q_r the amount of heat rejected through convective cooling. q_{gen} is updated at every time step to take into account any changes in the parameters that determine the cells' internal resistance (See Eq. (3)). The amount of heat rejection q_r is given by the temperature rise of the coolant air when passing through the flow channel [26],

$$q_r = \dot{m}_a C_{p,a}(T_{\text{mo}} - T_{\text{mi}}), \tag{5}$$

where $\dot{m}_a$ is the coolant air mass flow rate through each channel, $C_{p,a}$ the specific heat capacity of air, T_{mo} the bulk mean outlet air temperature, and T_{mi} the bulk mean inlet air temperature.

The present work considered a lumped thermal model approach for the sake of simplicity of analysis. The internal temperature gradient inside the single cell was assumed to be relatively small so that a single cell temperature T_{cell} can be used to represent the entire cell domain temperature. For the typical HEV system's cooling strategy, the measured temperature spread inside the single cell depicted in Fig. 3 during the cycling test is mostly lower than 1 °C.

The outlet air temperature T_{mo} is related to the cell temperature T_{cell} by the following equation under the constant wall (cell surface) temperature condition [26],

$$\frac{T_{\text{cell}} - T_{\text{mo}}}{T_{\text{cell}} - T_{\text{mi}}} = \exp\left(-\frac{PL}{\dot{m}_a C_{p,a}}\overline{h}\right), \tag{6}$$

where P is the wetted perimeter of the channel, and $\overline{h}$ the flow length average heat transfer coefficient. Plugging Eqs. (5) and (6) into Eq. (4), T_{cell} is expressed in an explicit form as follows.

$$m_{\text{cell}}C_{p,c}\frac{\mathrm{d}T_{\text{cell}}}{\mathrm{d}t} = q_{\text{gen}} - \dot{m}_a C_{p,a}(T_{\text{cell}} - T_{\text{mi}}) \tag{7}$$
$$\times \left[1 - \exp\left(-\frac{PL}{\dot{m}_a C_{p,a}}\overline{h}\right)\right].$$

By integrating the above equation with respect to time, T_{cell} can be found.

For laminar flow in ducts, available heat transfer coefficients under a variety of boundary conditions were well summarized by Shah and London [27]. In this model, the simultaneously developing laminar flow in parallel plates was considered. Note that the aspect ratio a/b for the channel in Fig. 4 is quite small so that rectangular channel can be treated as the parallel plate geometry without great loss of accuracy. Then the wetted perimeter is approximated as $P \approx 2b$. The closed form correlation for the flow length average Nusselt number in parallel plates with the constant wall temperature condition is given as.

$$\overline{Nu}_T = 7.55 + \frac{0.024L_*^{-1.14}}{1 + 0.0358Pr^{0.17}L_*^{-0.64}}, \tag{8}$$

where Pr is the Prandtl number, and L_* the dimensionless distance in the flow direction for the thermal entrance region heat transfer. L_* is given as,

$$L_* = \frac{L}{D_h RePr}, \tag{9}$$

$$D_h = \frac{4ab}{P} \approx 2a, \tag{10}$$

$$Re = \frac{\dot{m}_a D_h}{\mu(ab)}, \tag{11}$$

where D_h is the hydraulic diameter, Re the Reynolds number, and μ the dynamic viscosity of air. The convection heat transfer coefficient is defined as follows.

$$\overline{h} = \frac{k_a \overline{Nu}_T}{D_h}. \tag{12}$$

Here, k_a is the thermal conductivity of the coolant air. Temperature is then calculated by Eq. (7), using value of the convection heat transfer coefficient from Eq. (12).

The performance of thermal management system is often represented by thermal resistance R_{th}, which is defined as the temperature difference across the medium where the unit heat energy per second transfers through it. The smaller the thermal resistance is, the better thermal performance is. Since the cell is cooled by the forced convection in the air channel, the temperature difference between the cell and the inlet air is suitable to define the thermal resistance. At the steady state, Eq. (7) turns into as follows to express the thermal resistance.

$$R_{\text{th}} \equiv \frac{T_{\text{cell}} - T_{\text{mi}}}{q_{\text{gen}}} = \left[\dot{m}_a C_{p,a}\left(1 - \exp\left(-\frac{PL}{\dot{m}_a C_{p,a}}\overline{h}\right)\right)\right]^{-1} \tag{13}$$

Above equation implies that the thermal resistance depends on the geometry of the air channel and the amount of air flow rate, which are adjustable parameters according to the system's technical requirements such as the battery system size and the coolant pumping power. Once the thermal resistance is determined by Eq. (13), one can readily judge the degree of cooling performance by simply calculating T_{cell}.

3. Experimental

K-type thermocouples were used for temperature sensing with which an AGILENT data acquisition system (a 34,970 A 3-slot control unit and three 34,901 A 20-channel multiplexers) was used for data acquisition. Several thermocouples were attached to the battery cell surface, and the system voltage was also monitored for SOC and safety purposes.

The test chamber was a multi-purpose environmental chamber capable of controlling temperature and humidity. And a Toshiba 450 V electric cycler customized to run power and current cycles was used to provide electric loads on the battery. The inlet air temperature of the battery system was controlled by the designated chamber temperature. Two different electric loads were used for cycle test purpose. One was a square pulse current duty and the other was a root-mean-square (RMS) adjusted US06 equivalent cycle (30 A RMS, the cycle obtained from simulating US06 vehicle operation pattern).

A customized fan-blower (12 V–80 W) was used to provide air flow. Air flow rate was measured with a differential pressure type portable digital air flow-meter (Seoul Industry Engineering) capable of measuring flow rate in the range of 20–250 m³ h⁻¹ (CMH) with a possible error of 1%.

4. Results and discussion

4.1. Validation of the model

4.1.1. Comparison with square pulse current duty test result

To examine the accuracy of model predictions, a test rig similar to what was shown in Figs. 2 and 4 was constructed and cycle-tested. 40 A square pulse cycle (repetition of 10 s charge and 10 s discharge) was used for the purpose of easy comparison where the SOC was kept at 50%. Flow rates were set such that the flow rates per each channel are 2.5, 3.4, and 5.3 CMH. The inlet coolant air temperature was set to 35 °C. The values of 10-s direct current internal resistance were used for heat generation calculation.

The measured temperature traces under various given flow rates were shown in Fig. 5. Naturally, high flow rate of air gives rise to faster and better cooling effect on the cell. To predict the cell temperature under given conditions, convection heat transfer coefficients were calculated as a function of flow rate using Eq. (12) and inserted into Eq. (7). As compared in Fig. 5, the proposed model captures the dynamic temperature behavior very accurately for both transient and steady states. For a full prediction of the battery temperature under varying flow rate when fan control logic is fully operational, the model may be able to cover the entire feasible range of fan operating points.

For the current thermal management design, 4 to 5 CMH of flow rate per channel is desired to keep the maximum cell temperature below 40 °C when running with inlet air temperature of 35 °C under 40 A RMS or equivalent current duties.

4.1.2. Comparison with vehicle driving pattern test result

US06 simulated current cycle for the two-mode (electric vehicle mode and power assistance mode) HEV power usage was obtained, modified, and run with both the simulation model and test rig with batteries fabricated specifically for HEV use under the flow rate of 3.3 CMH per channel. The cycle was modified to have 30 A RMS duty from the original 40 A RMS for the current model-test result comparison's purposes. The inlet coolant air temperature was set to 30 °C and initial SOC was 50%.

To make a reasonable estimation of the heat generation, one of the most important factors is cell's internal resistance. The internal resistance values were obtained from DCPR of cells where the resistance values under 2-, 5-, 10- and 30-s power duration were measured as a function of temperature and SOC (see Table 1 for the 10-s internal resistance). Usually, 30-s resistance is larger than 10-s resistance by approximately 80–90%, and selection of duration to estimate internal resistance values for model prediction is of critical importance.

A single US06 current cycle lasts for 600 s. After the end of the fourth cycle, the same cell temperature trace was repeated with the temperature variation between 32 and 33 °C as shown in Fig. 6. For the model prediction, internal resistances with various pulse durations were examined, and the proper one for heating estimation under the real driving pattern was found to be 10-s resistance.

The internal resistance was continuously updated depending on SOC and temperature for the model, thus the heat generation rate was varied with actual test data. The present lumped thermal model with the temporally updated resistance values gave good results and reasonably followed the dynamic temperature traces of real system with the maximum difference of 1 °C as shown in Fig. 6.
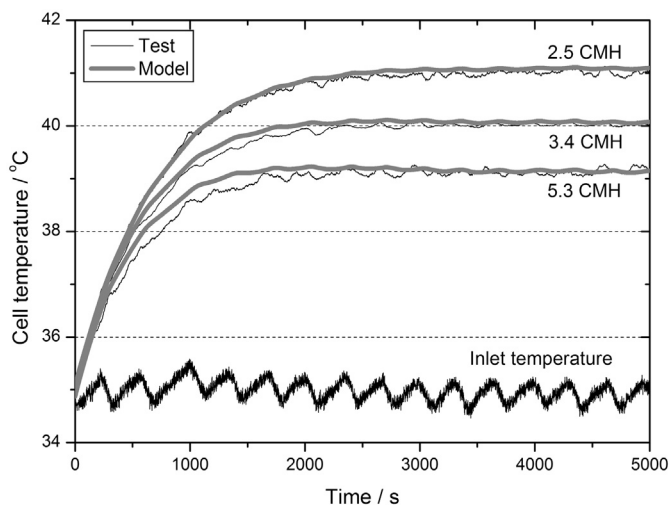

Fig. 5. Cell and inlet temperature measured per given flow rates under 40 A square pulse cycling and varying coolant flow rates and comparison with model predictions.
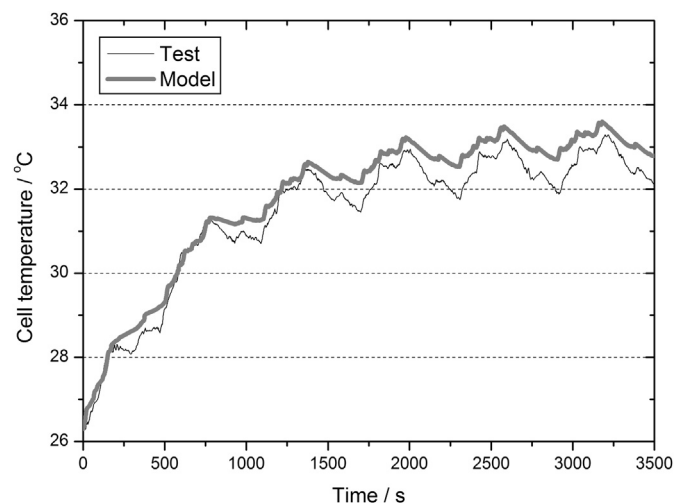

Fig. 6. Modeling results and comparison with test data. Adjusted US06 current profile is applied and the flow rate per channel is 3.3 CMH.

4.2. Parametric studies

In terms of the coolant flow system structuring and investigating the effects of design parameters at the early design phase of the system, the lumped thermal model can be utilized effectively. In the following sections, parametric studies were explored to see the effect of important design parameters such as the air channel width and the coolant flow rate. Dimensional parameters other than varying were based on the basic structure of Fig. 2. 40 A square pulse cycle was assumed as the current duty, and the cell temperature was calculated up to 45 °C, considering the temperature range where the internal resistance was measured.

4.2.1. Effect of air channel width

Dependencies of the cell temperature and the thermal resistance on the air channel width with varying coolant flow rates were shown in Fig. 7. Here, the coolant inlet temperature was 35 °C. Both the cell temperature and the thermal resistance tend to increase with widening of air channel under the constant coolant flow rate, due to the decrease of convection heat transfer rate between the cell and its neighboring coolant air. In other words,

although the overall air channel behaves as the entrance region of developing flow in the limit of sufficiently large air channel width, the heat transfer coefficient gradually decreases due to the fixed flow rate leading to slowdown of the free stream velocity near the surface.

In the opposite limit of extremely small channel width, the air flow is fully developed along the channel height and the Nusselt number becomes constant. Inserting Eq. (12) into Eq. (13) and setting $\overline{Nu}_T = 7.55$, the thermal resistance is expressed as.

$$R_{th} = \left[\dot{m}_a C_{p,a} \left(1 - \exp \left(-\frac{PLk_a}{\dot{m}_a C_{p,a} D_h} 7.55 \right) \right) \right]^{-1} \tag{14}$$

Dashed curves in Fig. 7 illustrated results from the above equation. As expected, the solid curve based on Eq. (13) and the dashed curve based on Eq. (14) coincide with each other in the small range of channel width while the differences between them become larger as the channel width increases. When relatively small air channel is allowable, e.g. $a \leq 3$ mm, to meet the system's size requirement, Eq. (14) could provide the early estimation of the cell temperature accurately. Considering the fact that the exponential term can be neglected as $a \rightarrow 0$, Eq. (14) can be further simplified as follows.

$$R_{th} \cong \frac{1}{\dot{m}_a C_{p,a}}; \quad a \rightarrow 0 \tag{15}$$

Above equation implies that only capacitive resistance plays a role in determining the overall thermal resistance in this limit, thus R_{th} becomes independent of the air channel width. It is worthwhile to note that the coolant air outlet temperature may approach the cell temperature when the air channel is extremely narrow, and thereby the convective resistance can be neglected, leaving only the capacitive term.

4.2.2. Effect of coolant flow rate

Predicted cell temperature and thermal resistance vs. coolant flow rate for different air channel width were shown in Fig. 8. The coolant inlet temperature was the same as before. The cell temperature and the thermal resistance decrease with increasing the coolant flow rate, though the decreasing amount is attenuated gradually for high flow rate. Based on this characteristic, increase of the flow rate should be settled in the certain range where the pumping power device, like a fan, could deliver its regular performance and the benefit of having high flow rate is not significant due to only the small amount of temperature decrease.

When it comes to the low flow rate range, both the cell temperature and the thermal resistance sharply increase, where the capacitive resistance becomes dominant factor determining thermal behavior. Especially, Eq. (14) would still be used to approximate thermal behavior in the low flow rate range, due to the fully developed characteristic. As shown in Fig. 8, Eq. (14) depicted by dashed curves estimates the cell temperature accurately within 1 °C when the flow rate lower than 6 CMH and the air channel smaller than 4 mm are considered.

When determining values of design parameters, it is worth considering the state of cell at the middle or end of life to keep the sufficient cooling performance during a whole lifetime of cell. In other words, since the internal resistance of the cell increases with time due to an aging effect, the amount of heat generation will go up in the same manner. Then proper values of design parameters should be selected in accordance with this varying heat generation, so that the cell temperature is maintained well under the target value during lifetime.
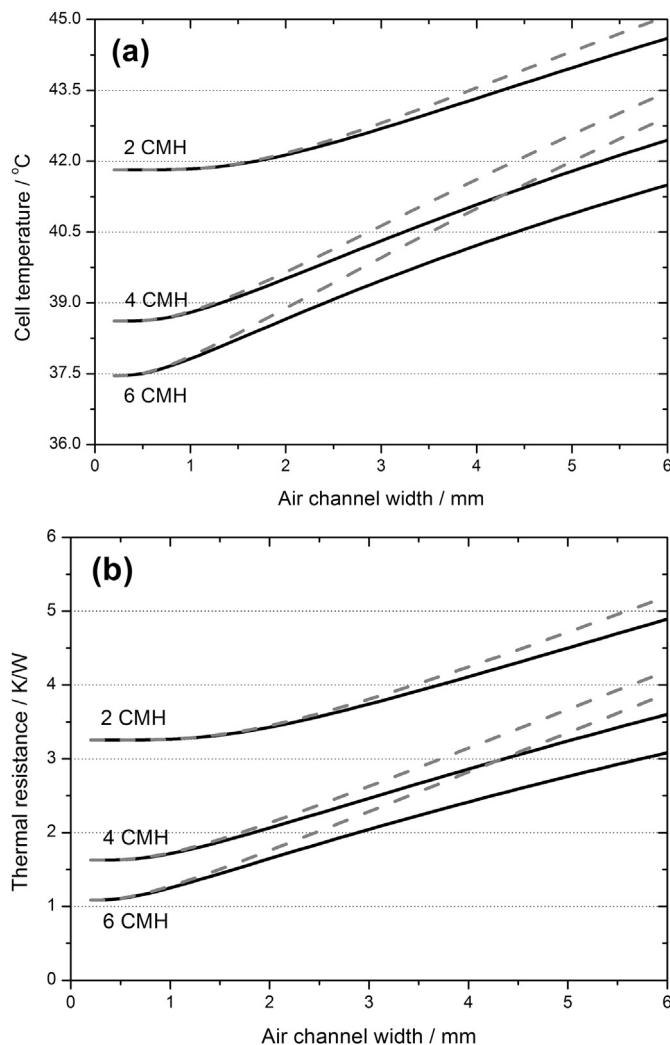

Fig. 7. Influence of the air channel width on (a) the cell temperature and (b) the thermal resistance with the different coolant flow rate.
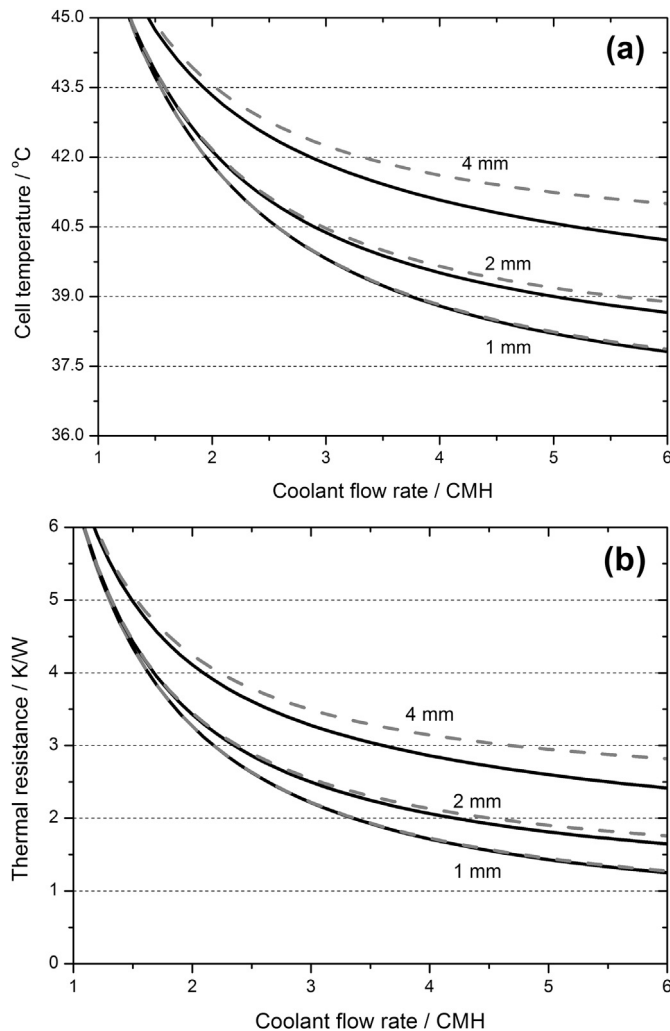
Fig. 8. Influence of the coolant flow rate on (a) the cell temperature and (b) the thermal resistance with the different air channel width.

5. Conclusion and future works

Design of thermal management system includes three basic parts, flow system modeling and estimation, flow system design and optimization, and building of fan operation strategy for air-cooled systems. The flow system modeling and estimation, and the flow system designing occur early in system design phases before mechanical system structuring. This is because it is, by experience, harder to change the duct shapes, fan performance (flow rate and static pressure), and etc., while the fan operation strategy and logic can be developed later in design phase. Generally flow structuring requires significant physical modification of the battery system.

The present work considered the very first part of the design; structuring the flow system for modeling and estimations. Based on the basic design concepts such as the channel size and cell mating (two-cell units), and also on the physical properties of the cells, efforts had been made to help expedite the battery system design. The test instrumentations were so designed that any abnormal conditions such as fluctuating ambient temperature and effects of humidity were excluded that direct comparison was reasonable for the currently presented work.

According to the modeling results and comparison with the test data, the following facts had been learned. The lumped thermal model gave excellent estimation of battery cell thermal behavior for the present battery system. The application of the classical heat transfer model of internal flow through parallel plates yielded the simple and explicit form of equation enabling the prediction of the dynamically varying cell temperature under a variety of design parameters. Use of internal resistance values updated according to the parameters such as charge/discharge status, SOC, and cell temperature was shown to reasonably predict the thermal behavior of the system under a dynamic operational condition − a US06 power cycling for two-mode HEV which is expected to cover 97% of all U.S. drivers' driving pattern and duty [28].

Effects of two important adjustable design parameters were also explored using the lumped thermal model. In case of small air channel width and limited amount of coolant flow rate approximations, the model was expressed in more simplified form, which was valid with reasonable accuracy when the typical magnitude of design parameters was selected.

Flow homogenization through each channel is an issue of critical importance though not covered in the present work. Failure to homogenize the flow through each channel, such that the flow rate distribution is uneven among channels, would cause another problem of temperature spread among cells in the battery system. This would result in uneven deterioration of cells and, eventually, makes it harder to monitor, control, and condition the battery system, which are critical for commercializing the system especially in terms of warranty and lifetime issues. After determining basic design parameters such as the air channel dimension and flow rate with the help of the lumped thermal model, inlet and outlet duct could be carefully designed enabling uniform flow rate around each cell.

Building fan operation strategy and logic is a work, in part, of the battery management system (BMS) development. Large amount of test efforts such as mapping the cooling capacity of battery system according to current loads, ambient and cell temperatures, and state of health (SOH) of cells, however, are required to complete this part of thermal management design.

References

[1] U. Kohler, J. Kumpers, M. Ullrich, J. Power Sources 105 (2002) 139–144.
[2] A. Du Pasquirer, I. Plitz, S. Menocal, G. Amatucci, J. Power Sources 115 (2003) 171–178.
[3] O. Bitsche, G. Gutmann, J. Power Sources 127 (2004) 8–15.
[4] C. Tatard, in: AIAA 21st International Communications Satellite System Conference Exhibition, 2003, pp. 2003–2232.
[5] K. Smith, C.Y. Wang, J. Power Sources 160 (2006) 662–673.
[6] H. Lee, H.-J. Kim, D. Kim, S. Choi, J. Power Sources 176 (2008) 359–362.
[7] G. Kim, A. Pesaran, R. Spotnitz, J. Power Sources 170 (2007) 476–489.
[8] A. Pesaran, D. Bharathan, G. Kim, A. Vlahinos, T. Duong, in: 21st Electric Vehicle Symposium, 2005.
[9] B. Scrosati, J. Garche, J. Power Sources 195 (2010) 2419–2430.
[10] M. Contestabile, M. Morselli, R. Paraventi, R.J. Neat, J. Power Sources 119 (2003) 943–947.
[11] J. Shim, R. Kostecki, T. Richardson, X. Song, K.A. Striebel, J. Power Sources 112 (2002) 222–230.
[12] K. Askura, M. Shimomura, T. Shodai, J. Power Sources 119 (2003) 902–905.
[13] S. Hossain, Y.-K. Kim, Y. Saleh, R. Loutfy, J. Power Sources 161 (2006) 640–647.
[14] E.P. Roth, D.H. Doughty, D.L. Pile, J. Power Sources 174 (2007) 579–583.
[15] C.Y. Wang, V. Srinivasan, J. Power Sources 110 (2002) 364–376.
[16] D.H. Doughty, P.C. Butler, R.G. Jungst, E.P. Roth, J. Power Sources 110 (2002) 357–363.
[17] P. Nelson, D. Dees, K. Amine, G. Henriksen, J. Power Sources 110 (2002) 349–356.
[18] A. Mills, S. Al-Hallaj, J. Power Sources 141 (2005) 307–315.
[19] S. Al-Hallaj, J.R. Selman, J. Power Sources 110 (2002) 341–348.
[20] S. Al-Hallaj, J.S. Hong, H. Maleki, J.R. Selman, J. Power Sources 83 (1999) 1–8.
[21] USABC/US DOE/INEEL, FreedomCAR Battery Test Manual for Power-assist Hybrid Electric Vehicles, October 2003.
[22] T.M. Bandhauer, S. Garimella, T.F. Fuller, J. Electrochem. Soc. 158 (2011) R1–R25.
[23] J.S. Hong, H. Maleki, S. Al-Hallaj, L. Redey, J.R. Selman, J. Electrochem. Soc. 145 (1998) 1489–1501.

[24] T. Ohshima, M. Nakayama, K. Fukuda, T. Araki, K. Onda, Electr. Eng. Jpn. 157 (2006) 17–24.
[25] H. Maleki, S. Al-Hallaj, J.R. Selman, R.B. Dinwiddie, H. Wang, J. Electrochem. Soc. 146 (1999) 947–954.
[26] F.P. Incropera, D.P. Dewitt, Fundamentals of Heat and Mass Transfer, fourth ed., John Wiley & Sons, 1996.
[27] R.K. Shah, A.L. London, Laminar Flow Forced Convection in Ducts, Academic Press, 1978.
[28] L. Nitz, in: Plug-in Hybrid Electric Vehicle Workshop, 23rd Electric Vehicle Symposium, 2007.

Nomenclature

a: width of air channel
b: height of air channel
$C_{p,a}$: specific heat capacity of air
$C_{p,c}$: specific heat capacity of cell
D_h: hydraulic diameter
$\overline{h}$: convective heat transfer coefficient
iR_{cell}: direct current internal resistance
I: electrical current
k_a: thermal conductivity of air

L: length of air channel
L_*: dimensionless length of air channel
$\dot{m}_a$: mass flow rate of air through each channel
m_{cell}: cell weight
$\overline{Nu}_T$: Nusselt number averaged over L
P: wetted perimeter of a channel
Pr: Prandtl number
q_{gen}: heat generation by cell
q_r: heat rejected through convection
Re: Reynolds number
R_{th}: thermal resistance
T_{cell}: cell temperature
T_{mi}: inlet (ambient) mean temperature
T_{mo}: outlet mean temperature
U: cell open circuit voltage
V: cell voltage

Greek symbols

μ: dynamic viscosity of air
τ: charge/discharge pulse duration